Syntenin, a syndecan adaptor and an Arf6 phosphatidylinositol 4,5-bisphosphate effector, is essential for epiboly and gastrulation cell movements in zebrafish

Kathleen Lambaerts[1], Stijn Van Dyck[1], Eva Mortier[1], Ylva Ivarsson[1], Gisèle Degeest[2], Annouck Luyten[1], Elke Vermeiren[1], Bernard Peers[3], Guido David[2] and Pascale Zimmermann[1,*]

[1]Laboratory for Signal Integration in Cell Fate Decision, [2]Laboratory for Glycobiology and Developmental Genetics, Department of Human Genetics and VIB, K.U.Leuven, B-3000 Leuven, Belgium
[3]Laboratoire de Biologie Moléculaire et de Génie Génétique, Université de Liège, B-4000 Liège, Belgium
*Author for correspondence (pascale.zimmermann@med.kuleuven.be)

Accepted 28 October 2011
Journal of Cell Science 125, 1129–1140

doi: 10.1242/jcs.089987

Summary

Epiboly, the spreading and the thinning of the blastoderm to cover the yolk cell and close the blastopore in fish embryos, is central to the process of gastrulation. Despite its fundamental importance, little is known about the molecular mechanisms that control this coordinated cell movement. By a combination of knockdown studies and rescue experiments in zebrafish (*Danio rerio*), we show that epiboly relies on the molecular networking of syntenin with syndecan heparan sulphate proteoglycans, which act as co-receptors for adhesion molecules and growth factors. Furthermore, we show that the interaction of syntenin with phosphatidylinositol 4,5-bisphosphate (PIP2) and with the small GTPase ADP-ribosylation factor 6 (Arf6), which regulate the endocytic recycling of syndecan, is necessary for epiboly progression. Analysis of the earliest cellular defects suggests a role for syntenin in the autonomous vegetal expansion of the yolk syncytial layer and the rearrangement of the actin cytoskeleton in extra-embryonic tissues, but not in embryonic cell fate determination. This study identifies the importance of the syntenin–syndecan–PIP2–Arf6 complex for the progression of fish epiboly and establishes its key role in directional cell movements during early development.

Key words: Syntenin, Syndecan, Arf6, PIP2, Zebrafish, Epiboly, Yolk syncytial layer

Introduction

Gastrulation is an early phase of vertebrate development during which cells undergo coordinated movements to organize the three primary germ layers of ectoderm, mesoderm and endoderm and to establish the body axes of the embryo (Leptin, 2005). In zebrafish, the zygote lies on top of the so-called 'yolk cell', which feeds the developing embryo, and undergoes meroblastic cleavage to generate a blastoderm cap on this yolk cell. The first coordinated cell movement occurs after the ninth or tenth zygotic cell division, and is called epiboly. Epiboly is visualized as the thinning and the spreading of the blastoderm over the yolk. Epiboly begins when the vegetally localized large yolk cell domes into the blastoderm, which is initially present at the animal pole. It ensues when the dividing blastoderm cells spread, thin over and eventually enclose the yolk cell – corresponding to 100% epiboly (Rohde and Heisenberg, 2007; Solnica-Krezel, 2006; Warga and Kimmel, 1990). Halfway through epiboly, a second movement resulting in the internalization of the marginal blastomeres gives rise to the epiblast and the hypoblast – the latter representing the presumptive mesendoderm. Concomitantly with blastoderm internalization, the internalized cells and the non-involuting cells converge towards the dorsal side where they intercalate, resulting in a thickening and an extension of the dorsal axis. This process is referred to as convergent extension (Rohde and Heisenberg, 2007; Solnica-Krezel, 2005).

At the onset of epiboly, the blastula is composed of three cell layers: (1) the enveloping layer (EVL), a protective simple epithelium that is attached to the yolk cell by its vegetal rim; (2) the deep layer, which is covered by the EVL, containing the deeper blastomeres or deep cells that give rise to the embryo proper; and (3) the yolk syncytial layer (YSL). The EVL is referred to as an extra-embryonic tissue, but is formed by the outermost layer of blastoderm in the blastula. The YSL is also an extra-embryonic tissue that originates from the fusion of the most vegetal, nucleated blastoderm cells with the underlying yolk cell (D′Amico and Cooper, 2001; Kimmel et al., 1995). The yolk cell cytoplasm is thus invaded by animal cells and populated by their nuclei, the yolk syncytial nuclei (YSN), in which gene transcription occurs. A substantial number of the YSN are at the external edge of the YSL (eYSL), which is the part of the yolk cell cytoplasm located just beneath the blastoderm rim. The eYSL separates the vegetal, thin anuclear layer of yolk cell cytoplasm (YCL) from the inner YSL (iYSL), which is covered by the blastoderm. The YSL has inductive and patterning functions during early embryonic development. The dorsal part of the YSL functions similarly to the amphibian Nieuwkoop center; YSL signals induce endoderm, ventrolateral and head mesoderm, and control heart morphogenesis in zebrafish (Carvalho and Heisenberg, 2010; Lepage and Bruce, 2010).

Journal of Cell Science

In *Fundulus heteroclitus*, another teleost, disruption of the tight junctions between the YSL and the EVL causes the blastoderm to retract and accelerates the epiboly progression of the YSL, which emphasizes the active participation of the YSL in pulling the EVL and the deep cells towards the vegetal pole (Trinkaus, 1951). Endocytosis confined to the region of the eYSL, ensuring the disappearance of the surface of the yolk cell that is just peripheral to the advancing margin of the blastoderm, has been proposed to play a major role in epiboly (Betchaku, 1986). Other studies propose that the cytoskeleton of the YSL is a crucial component of epiboly. The YSL extends arrays of microtubules into the YCL and contains, after 50% epiboly, a contractile F-actin band. The disruption of the organization of these microtubules or microfilaments impairs epiboly (Cheng et al., 2004; Koppen et al., 2006; Solnica-Krezel and Driever, 1994; Strahle and Jesuthasan, 1993). Despite the crucial role of the YSL in the early development of teleost fish embryos, the molecular mechanisms underlying YSL morphogenesis and coordinated movement are still not well understood (Carvalho and Heisenberg, 2010; Lepage and Bruce, 2010).

Scaffold proteins impact the spatial–temporal dynamics of signaling complexes. Syntenin is a small intracellular scaffold protein that contains two PSD-95, Discs-large, ZO-1 (PDZ) domains. These domains are well known for interacting with the C-terminal tails of transmembrane receptors (Nourry et al., 2003). Several types of proteins, including B-ephrins, Delta-1 and Frizzled were identified as binding partners for the PDZ domains of syntenin (Beekman and Coffer, 2008). Of particular relevance for the present study, syntenin was originally identified as a binding partner for the syndecan family of heparan sulphate proteoglycans (Grootjans et al., 1997). Syndecans are common at the cell surface and function as co-receptors for numerous adhesion molecules and growth factors, some of which, such as FGFs and Wnt proteins, are morphogens (Lambaerts et al., 2009). A mechanistic study in cultured cells showed that syntenin functions as a rate-limiting factor for the recycling of endosomal syndecans to the plasma membrane (Zimmermann et al., 2005). This recycling pathway is important for cell spreading, at least in cell culture, and depends on the activation of the small GTPase ADP-ribosylation factor 6 (Arf6), which recruits the phosphatidylinositol-4-phosphate 5-kinase on perinuclear endosomes, and on the ability of syntenin to directly interact with phosphatidylinositol 4,5-bisphosphate [PtdIns(4,5)P_2 or PIP2].

Here we aimed to clarify whether and when syntenin is relevant in vivo and investigated its role in zebrafish. We found that syntenin is essential for gastrulation movements. Its downregulation primarily affects early embryonic cell movements, and specifically, the epiboly movement of the YSL. Syndecans were found to be essential for epiboly initiation slightly earlier than syntenin. The epiboly defects observed in syntenin morphant fish embryos correlate with anomalies of the YSL actin cytoskeleton, strictly depend on the Arf6–PIP2 pathway and depend to some extent on syndecans. We propose that the syntenin–syndecan–PIP2–Arf6 complex functions in the fish embryo YSL to control directional progression during epiboly.

Results

Syntenin is essential for the progression of epiboly and convergence extension movement

We found two genes encoding syntenin (*sdcbp*) in zebrafish. Corresponding protein sequences were deduced from the cDNAs, and were referred to as syntenin-a and syntenin-b (supplementary material Fig. S1A). RT-PCR revealed that both *syntenin-a* and *syntenin-b* transcripts are maternally supplied and that expression persists during gastrulation (Fig. 1A). S*yntenin-a* and *syntenin-b* transcripts were detected throughout the embryo by whole-mount in situ hybridization (WISH) at the two-cell stage and during blastula and gastrula stages (supplementary material Fig. S1B,C).

To investigate the function of syntenin during embryonic development, two different morpholino oligonucleotides, targeting the translation start site in *syntenin-a* transcripts (MOsynta and MOsyntabis) were designed. Both MOsynta and MOsyntabis effectively inhibited in vitro synthesis of syntenin-a, whereas similar amounts of mismatch morpholino had no effect (supplementary material Fig. S1D). Morpholinos generally produce a range of effects that represent reduced gene function. Only 15% of the embryos (of a total of 87 embryos) injected with 6 ng MOsynta survived 24 hours post fertilization (h.p.f.) (Fig. 1B). Close examination showed that syntenin-a-deficient embryos initiate epiboly, progress to 50% epiboly, and cells undergo internalization (Fig. 1C,D, black arrowhead) similarly to control (non-injected or mismatch-injected) embryos. However, shield formation (Fig. 1D, white arrowhead) was delayed or absent in most morphants. At 8 h.p.f., when the blastoderm covered 75% of the yolk in controls, most syntenin-a morphants were at 50% epiboly. At 10 h.p.f., although epiboly was complete in controls, syntenin-a morphants showed no further progression of epiboly (Fig. 1C,D).

The delay in formation of the embryonic shield, morphologically defined as a discrete group of cells at the dorsal side of the germ ring, suggested defective convergence movements in syntenin-a morphants (Fig. 1, compare C and D, white arrow). Complementary experiments confirmed a role for syntenin-a in convergent extension movements. Surviving syntenin-a morphants exhibited a shorter body axis compared with controls (Fig. 1E). WISH on morphant embryos with complete epiboly, revealed a shortened and broadened notochord (no tail, *Ntl*) and a widening of the presomitic mesoderm (paraxial protocadherin, *papc*) (Fig. 1F).

To quantify the epibolic defect, we distinguished four different categories of syntenin-a morphants on the basis of their epiboly progression at 10 h.p.f. Embryos with 100% yolk coverage were considered normal. Embryos displaying more than 85%, between 85 and 60%, and less than 60% coverage of the yolk were grouped as class I, class II and class III, respectively (Fig. 1G, top panels). Using this classification, we established that the severity of the defect in epiboly increases with the dose of morpholino. More than 90% of the embryos (n=593) injected with 6 ng MOsynta were delayed in their epiboly, 78% qualifying as class III. Injection of 4, 2 or 1 ng MOsynta induced epibolic defects in 93, 29 or 10% of the embryos (n=221, 171 and 326), respectively, and 53, 4 or 1% ranked as class III. Similar defects were observed for MOsyntabis (Fig. 1G). To verify that the epiboly effects were due to specific interference with *syntenin-a* expression and function, we co-injected *syntenin-a* RNA (synta RNA), which encodes wild-type protein but mutated such that MOsynta binding is prevented. Co-injection of 50 pg of synta RNA, a dose that has no influence on zebrafish embryogenesis, with 6 ng MOsynta significantly decreased the percentage of embryos with epibolic delay (30% versus 92%) and the incidence of class III defects (13% versus 78%) (Fig. 1G). Together, these results indicate that syntenin-a is required for epiboly progression and convergent extension during zebrafish development.

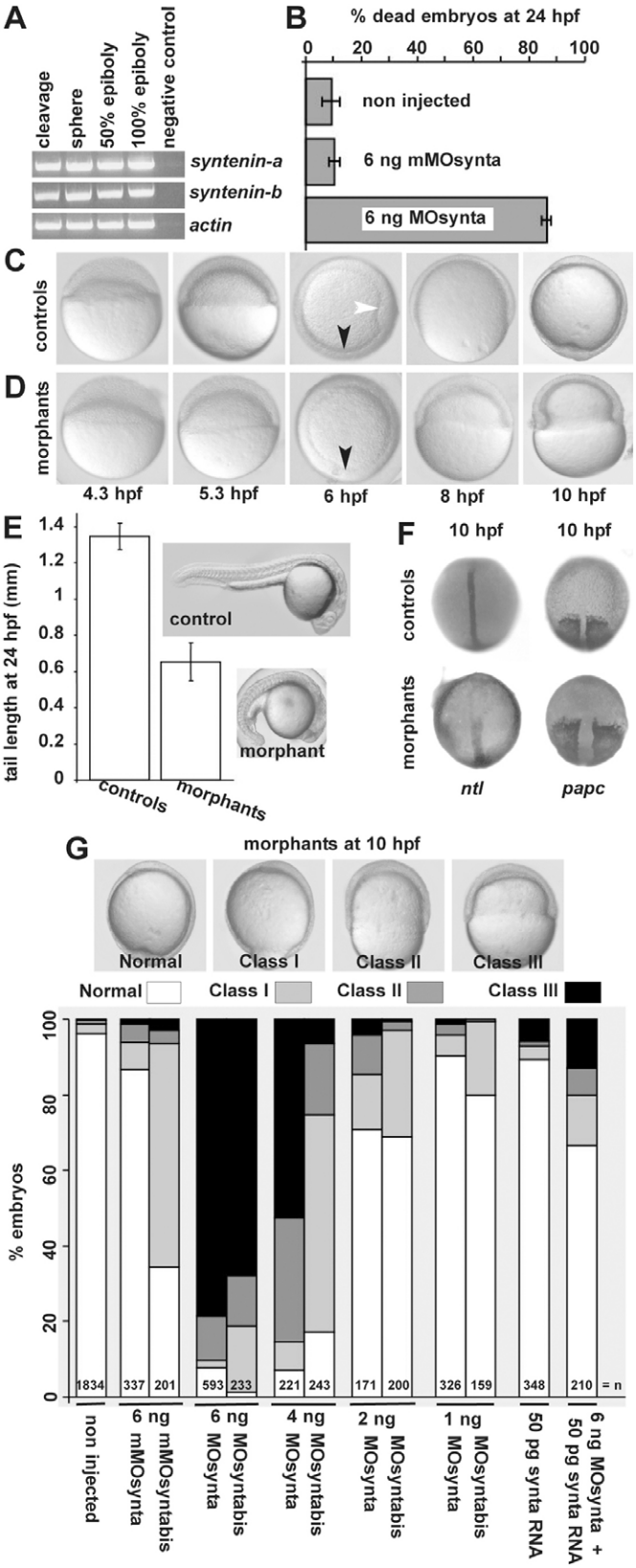

Syntenin knockdown does not affect the differentiation, division or viability of embryonic cells

We examined whether syntenin-a is important for embryonic patterning and/or cell differentiation in the severely affected morphants. Efficient knockdown of syntenin-a does not prevent the establishment of the dorso-ventral axis as demonstrated by the normal (dorsal) expressions of the patterning genes chordin and goosecoid at 4.7 h.p.f. (Fig. 2A). It also does not compromise cell fate determination, as syntenin-a-morphants display expressions of markers specific for ectoderm (*fkd3*), mesoderm (*ntl*) or endoderm (*gata5*) at 6 h.p.f. (Fig. 2B). Immunostaining for phosphorylated histone H3 (Fig. 2C) and BrdU incorporation experiments (data not shown) did not reveal defects in cell division at early gastrulation. Also acridine orange experiments did not reveal a significant increase in the number of dying cells in morphants (Fig. 2D). Staining for β-catenin at 6 h.p.f. indicated that the embryonic cells remain in contact with each other (data not shown). We then specifically examined the EVL and the YSL. Visualizing of the EVL, by WISH using *krt8* probes, also confirmed a migration block at the equator of the embryo (Fig. 3A). Tracing the YSN and the cytosol of the YSL in living embryos, using sytox green and GFP, respectively, further confirmed that these structures are blocked in their epibolic progression. At 5.3 h.p.f., the YSN were dispersed uniformly at the margin and below the blastoderm in both controls and morphants. However, at 9 h.p.f., the YSN and the YSL front were still located near the equator in syntenin-a morphants, whereas those of controls covered 90% of the yolk (Fig. 3B,C). Taken together, these data indicate that syntenin-a is essential for the progression of the epiboly of embryonic and extra-embryonic cells from the equator to the vegetal pole.

Effects of syntenin knockdown on the cytoskeleton

The role of syntenin-a in epiboly was further investigated by analyzing different mechanisms known to support epibolic progression. Endocytosis limited to a narrow ring of the eYSL, localized vegetally to the EVL rim and migrating front of the blastoderm, has been proposed to drive epiboly of the surface of the YSL and of the EVL that is tightly attached to it (Betchaku, 1986; Cheng et al., 2004; Solnica-Krezel and Driever, 1994).

Fig. 1. Effects of syntenin-a depletion on zebrafish early embryonic development. (**A**) Detection of transcripts encoding syntenin-a, syntenin-b and actin by RT-PCR at different stages of development. (**B**) Mortality at 24 h.p.f. upon injection of *syntenin-a* morpholino (MOsynta) but not mismatch morpholino (mMOsynta). (**C**,**D**) Epiboly in embryos injected with 6 ng MOsynta (D), compared with controls injected with 6 ng mMOsynta (C). Morphants develop normally to 50% epiboly, undergo internalization of the mesendodermal cells (presence of the germ ring, black arrowheads) but show severe defects in epiboly at later stages. White arrowhead indicates the shield in controls. (**E**) Comparison of tail lengths in controls and syntenin-a morphants injected with 1 ng MOsynta. Error bars indicate s.d. from the means. (**F**) Dorsal views of embryos showing the reduction in convergent extension in morphants, at 100% epiboly. (**G**) Illustration of the different classes of epibolic defects in syntenin-a morphants, at 10 h.p.f. (upper part). Images correspond to lateral views, except at 6 h.p.f., where animal pole views are shown. Histogram shows the quantification of the epibolic defects. Note that epibolic defects are observed with two independent morpholinos, are dose-dependent, and that *syntenin-a* RNA (synta RNA) co-injection corrects epibolic progression, illustrating the specificity of the morpholino effects. Values were obtained from at least three independent experiments; *n*, total number of embryos.

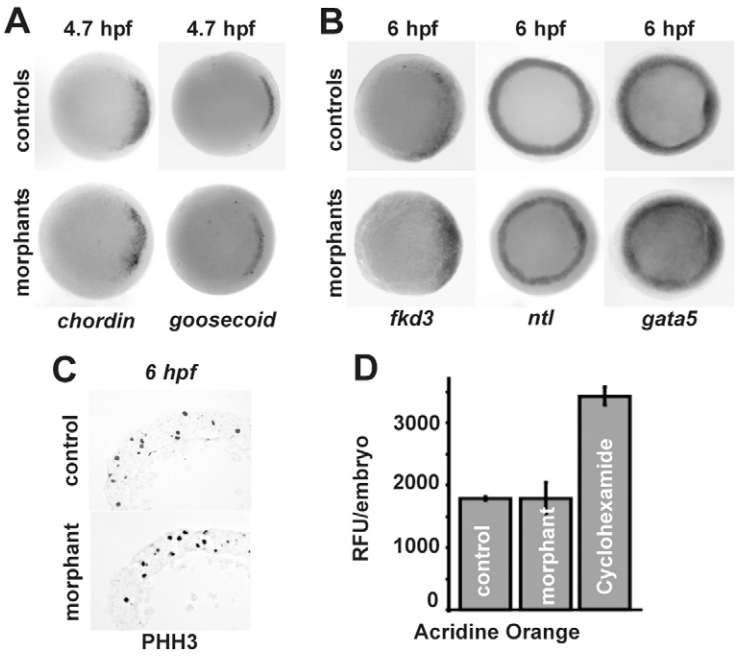

Fig. 2. Depletion of syntenin-a does not affect cell differentiation, proliferation or viability. (**A**,**B**) Animal pole views from WISH experiments illustrating the dorso-ventral patterning (A) and the differentiation (B) of embryonic tissues at the indicated time of development. Note the similarities between controls and morphants with blocked epiboly. (**C**) Transverse sections of embryos labelled with antibody against phosphorylated histone H3 (PHH3) illustrating cell division in controls and morphants. (**D**) Analysis of cell death, by Acridine Orange labelling, in living embryos at 6 h.p.f. Values correspond to the means of relative fluorescent units (RFU) per embryo. Error bars indicate s.d. from the means. Cycloheximide-treated embryos were used as positive controls.

Rhodamine–dextran uptake assays at shield stage in morphants yielded a circumferential staining, suggesting the endocytic process is functional (supplementary material Fig. S2). Progression of YSL epiboly is also dynamically regulated by pulling microtubule arrays, originating within the YSL and extending through the YCL to the vegetal pole (Solnica-Krezel and Driever, 1994; Strahle and Jesuthasan, 1993). Anti-tubulin staining of whole-mount syntenin-a morphants at 8 h.p.f. revealed no tubulin-free areas in the YCL (data not shown), unlike what has been reported for other epiboly-affected mutants (Lachnit et al., 2008). Although subtle differences in microtubule architecture might be missed, confocal analysis at 6 h.p.f. revealed that microtubule formation is similar in morphants and controls (Fig. 3D). After 50% epiboly, a punctate contractile actin band forms in the eYSL, and actin constriction has been claimed to support epiboly (Cheng et al., 2004; Koppen et al., 2006). Whole-mount Rhodamine–phalloidin staining was used to assess actin organization. At the shield stage, actin was present in the YSL of syntenin-a morphants, but in a disorganized manner when compared with the band of punctate F-actin in controls ($n=10$) (Fig. 3E, compare middle with left micrograph). However, constriction occurred (Fig. 3E, right), which is suggestive of a cell movement problem rather than a contraction problem. To further investigate the epiboly defects related to the YSL, we performed transmission electron microscopy at 6 h.p.f. No obvious difference in YSL structures could be observed at this stage. Also, the junctions between the eYSL and the EVL looked normal (Fig. 3F). Investigation of the EVL cells in syntenin-a morphants showed that these developed protrusions in which actin seems to accumulate, given the ruffled appearance of the cell borders. Such protrusions became more evident at 8 h.p.f. (Fig. 3G). Interestingly, the EVL cells appeared rounded in the morphants compared with the elongated shape observed in the controls (Fig. 3H). This suggested that tensile forces exerted by the YSL, and necessary for progression of epiboly, are deficient. Taken together, these data show that knockdown of syntenin-a affects the actin organization of the YSL and the EVL.

Syntenin-a is necessary for the autonomous movement of the YSL

Autonomous movement of the YSL is essential for the progression of epiboly (Trinkaus, 1951). Because we detected *syntenin-a* transcripts (Fig. 4A) and syntenin protein (Fig. 4B) in the YSL, we investigated whether depleting syntenin-a solely in the YSL would be sufficient to disturb epibolic progression. For this, MOsynta or MOsyntabis were co-injected with Rhodamine dextran into the YSL at sphere stage, when the YSL can be distinguished for injection and when morpholinos no longer freely diffuse to the rest of the embryo. Embryos showing Rhodamine fluorescence solely in the YSL were further examined. At 10 h.p.f., YSL syntenin-a morphants displayed a clear reduction in the progression of epiboly compared with mismatch-injected controls. Although epiboly had progressed up to around 90% in embryos with a mismatch-injected YSL ($n=37$ for mMOsynta and $n=62$ for mMOsyntabis), it stalled around 50% when the YSL had been injected with 6 ng MOsyntabis ($n=56$), and around 70% when injected with 3 ng MOsynta ($n=34$) (Fig. 4C). We then tested whether syntenin-a-regulated signaling from the YSL influences convergent extension of the deep cells. For this, we depleted syntenin-a solely in the YSL, and then analyzed convergent extension of the deep cells. At 10 h.p.f., YSL-injected morphants had formed a well-structured axis on incompletely covered yolk cells. Patterns of *ntl* and *papc* expression confirmed that YSL-depleted embryos formed notochord cells in the midline and also presomitic mesoderm. A well-structured axis was not observed in morphant embryos injected at the one-cell stage (Fig. 4D). This indicates that the deep cells of embryos where syntenin-a has been knocked down solely in the YSL are still able to perform convergent extension, even when the deep cells are blocked in their epiboly. Taken together, these results show that syntenin-a is required for epiboly

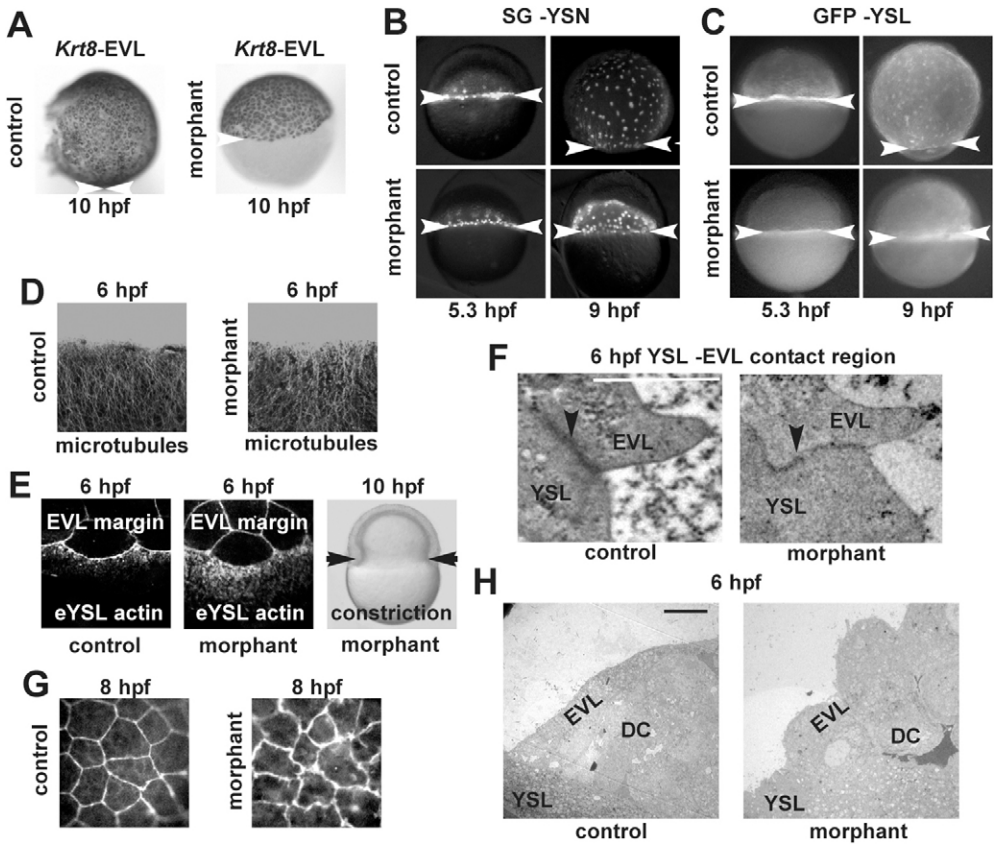

Fig. 3. Syntenin-a regulates the epiboly of the EVL and the YSL and impacts their cytoskeleton. (**A**) WISH at 10 h.p.f., using the *krt8* probe, illustrating the epibolic arrest of the EVL in class III syntenin-a morphants. (**B**,**C**) Fluorescence micrographs of embryos injected at 4 h.p.f. with Sytox Green (B) or GFP RNA (C) into the YSL, and observed at 5.3 h.p.f. and 9 h.p.f. Note the block of YSN (B) and YSL (C) progression in syntenin-a morphants. (**D**) Images corresponding to superimposed Z-stacks obtained by confocal microscopy with antibodies against tubulin and illustrating that the tubulin network is similar in controls and syntenin-a morphants at 6 h.p.f. (**E**) Confocal micrographs (left and middle) showing Rhodamine–Phalloidin staining of punctate actin band present in the eYSL. Note that the actin band in syntenin-a morphants displays a broadening. However, constriction can occur as shown in right image, black arrows. (**F**) Transmission electron micrograph of the contact region between EVL and YSL (black arrowhead). Well-defined EVL–YSL junctions are observed in both control and morphant. Scale bar: 1 μm. (**G**) Confocal micrographs of the actin architecture in the EVL by Rhodamine-Phalloidin staining at 8 h.p.f. illustrating that EVL cells in syntenin-a morphant display irregular shapes and multiple protrusions (white arrows). (**H**) Transmission electron micrographs showing the roundness of the EVL cells in morphants compared with controls. Scale bar: 10 μm. White arrowheads indicate the margin of the EVL (A), YSN (B) and YSL (C).

movement and acts on the autonomous epiboly process of the YSL.

Syndecans are important for the initiation of epiboly, and syntenin–syndecan interaction supports epiboly progression

Syntenin was originally identified as an intracellular partner for the syndecans (Grootjans et al., 1997). Syndecans are abundant cell-surface heparan sulphate proteoglycans that control cell migration, adhesion, proliferation and differentiation (Lambaerts et al., 2009). Because of their intrinsic affinity and abundance, syndecans appear to be preferential binding partners for syntenin and to be major players in the biological effects of syntenin (Grootjans et al., 2000). Therefore, we tested for a functional relationship between syntenin and syndecan during zebrafish epiboly.

Syndecan-1 is not present in zebrafish. Partial cDNA sequences found in public EST databases suggested the expression of its closest homolog, syndecan-3 (supplementary material Fig. S3). Orthologs for syndecan-2 and syndecan-4 were described in previous studies (Chen et al., 2004; Whiteford and Couchman, 2006). The cytoplasmic domains of the syndecans, and in particular their PDZ-binding motifs are conserved in zebrafish (Fig. 5A) consistent with their important signaling function (Lambaerts et al., 2009). Yet in zebrafish syndecan-4, an isoleucine substitutes the phenylalanine characteristic for the syndecan EFYA PDZ-binding motif. Although one can predict EIYA to be a good PDZ binding motif, the substitution might change the repertoire of PDZ-interacting proteins (Nourry et al., 2003). Ligand-overlay experiments indicated that syntenin-a binds all three zebrafish syndecans (Fig. 5B, left), whereas syntenin-b fails to interact with zebrafish syndecan-4 (supplementary material Fig. S4A). The syndecan-4 binding data were confirmed by surface plasmon resonance (Fig. 5B, right). Thus in zebrafish, there is no syndecan-1 but the three other syndecans are present and interact with syntenin-a. Syndecan-4, which displays a slightly different PDZ-binding motif, does not interact with syntenin-b.

All syndecans are ubiquitously expressed through early embryonic stages, as detected by RT-PCR (Fig. 5C) and WISH

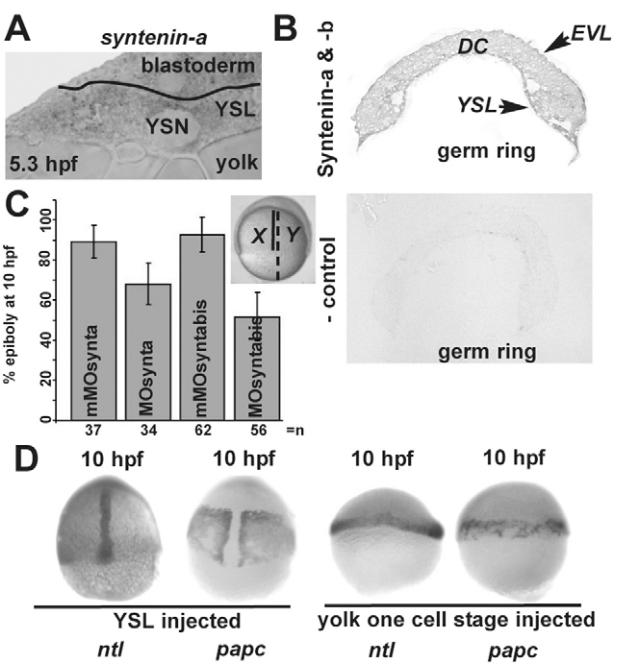

Fig. 4. Syntenin-a regulates the autonomous expansion of the YSL. (**A**) WISH section of an embryo at germ ring stage, stained with *syntenin-a* probe. (**B**) Immunohistochemical detection of syntenin-a and syntenin-b, at germ ring stage, showing the presence of the protein in the YSL, the deep cells (DC) and the EVL (top). Control reaction, obtained in the absence of primary antibody is shown below. (**C**) Measure of epiboly at 10 h.p.f., after injection of different morpholinos in the YSL at 4 h.p.f. The inset shows a morphant embryo at 10 h.p.f. after depletion of syntenin-a solely in the YSL by MOsynta. The percentage of epiboly was calculated by dividing the distance between the animal pole and the blastoderm margin (*X*) by the distance between the animal pole and the vegetal pole (*Y*), as illustrated in the inset. Error bars indicate s.d. from the means obtained in three independent experiments; *n*, total number of embryos. Note the delay in epiboly progression observed after injection of MOsynta or MOsyntabis, compared with mismatch morpholinos (mMOsynta and mMOsyntabis). (**D**) WISH micrographs of Class III embryos injected with MOsynta solely in the YSL at 4 h.p.f. (left) or in the yolk at one-cell stage (right) showing the distribution of *ntl* and *papc* probes. Note that YSL-injected morphants undergo convergent extension of the deep cells, despite the block of epiboly, whereas totally injected embryos are blocked in both processes. Images correspond to lateral views except in D (left), where they are dorsal.

(supplementary material Fig. S4B). We documented the effects of morpholinos directed against sequences overlapping with the syndecan ATG translation start sites, i.e. MOsdc2, MOsdc3 and MOsdc4, each of which is effective in vitro (supplementary material Fig. S4C). Injection of 6 ng of MOsdc2 caused epiboly defects at 10 h.p.f., but these were milder than in syntenin-a morphants, 58% of the embryos ($n=264$) presenting epiboly delay, but less than 1% of class III (Fig. 5D). Lower doses of morpholino were less effective. Higher doses were not used, because we found that gastrulation movements, and in particular epiboly, tended to be delayed in a non-specific manner when injecting higher doses. Injection of 6 ng of MOsdc3 ($n=144$) or MOsdc4 ($n=188$) induced drastic epiboly defects (Fig. 5D). Most defects were classified as class III (less than 60% epiboly; see Fig. 1G), but in the majority of the cases, the blastoderm remained completely on top of the yolk, indicating that these embryos did not initiate epiboly (Fig. 5D, micrograph). The effects were dose dependent when using 1–6 ng of morpholino (Fig. 5D). When co-injected, sub-optimal doses of the different sdcMO synergized in inducing epiboly defects (Fig. 5, compare E with D). This indicates that syndecans work together to control epiboly, and that syndecan-3 and syndecan-4 are essential for the proper initiation of epiboly, thus at an earlier stage than syntenin-a.

To investigate the role of syntenin-a–syndecan interaction during epiboly, we first tested whether injection of synta RNA could rescue epibolic defects observed with combined sub-optimal doses of sdcMO. No rescue of any class of morphants could be observed, indicating that overproduction of syntenin-a does not result in the stimulation of the residual activity of individual endogenous syndecans (Fig. 5E). We therefore tried to clarify the importance of the syntenin-a–syndecan interaction in epiboly by alternative approaches. We constructed a syntenin-a that was defective for syndecan binding (Δsdc), by mutating the carboxylate binding loop and the αB helix of the PDZ2 domain. Similar mutations in human syntenin (Grootjans et al., 2000) affect syndecan binding (see supplementary material Fig. S1A for the position and conservation of the residues). As expected, these mutations also affect all syndecan–syntenin-a interactions (Fig. 5B, left, middle panel). In overexpression studies, Δsdc-synta RNA resulted in a significant number of class I epiboly defects, which was not observed with wild-type synta RNA (Fig. 5F). This suggested that the mutant somehow works as a mild dominant-negative in terms of epiboly. Of course, owing to the intrinsic promiscuity of PDZ interactions (Nourry et al., 2003), one cannot exclude the idea that the mutations affect the interaction of syntenin-a with other cognate transmembrane receptors, but so far none of these were reported to function in epiboly (see also the Discussion). Intriguingly, in rescue experiments, Δsdc-synta RNA supported a partial rescue of the syntenin-a morphant phenotype (Fig. 5F). However, the mutant was never as potent as wild-type syntenin-a, suggesting that either the residual syndecan-binding activity of the mutant suffices to support the function or/and that syntenin-a interactions not affected by these mutations are also important for syntenin-a function in epiboly. Finally, we co-injected 1 ng of MOsynta with sub-optimal doses of each of the sdcMO, and scored for defects at 10 h.p.f. We observed additive effects for co-injections with sdc2 or sdc3 morpholinos. When sdc4 morpholinos were used, we observed a mild but significant synergistic effect (Fig. 5G). These effects were not due to the amount of MO injected, because similar effects were not induced by the same amount of corresponding mismatch morpholino (Fig. 5G). Together, the data point to a contribution of syndecans, and in particular syndecan-4, in syntenin-a function during epiboly.

Syntenin interacts genetically with Arf6, and directly with PIP2, to control epiboly

Syntenin was shown previously to mediate the recycling of the syndecans and syndecan cargo from ADP-ribosylation factor 6 (Arf6) perinuclear endosomes to the plasma membrane and thereby to support cell spreading in vitro (Zimmermann et al., 2005). We therefore examined whether Arf6 has a role in epibolic migration. We identified two zebrafish *arf6* orthologs, encoding Arf6-a and Arf6-b, both of which were identical to the human Arf6 protein except for one amino acid. We found, by RT-PCR, that *arf6* transcripts are maternally expressed and persist during zebrafish gastrulation (Fig. 6A). Arf6-a and Arf-b morpholinos had mild effects on epiboly, even when tested in combination

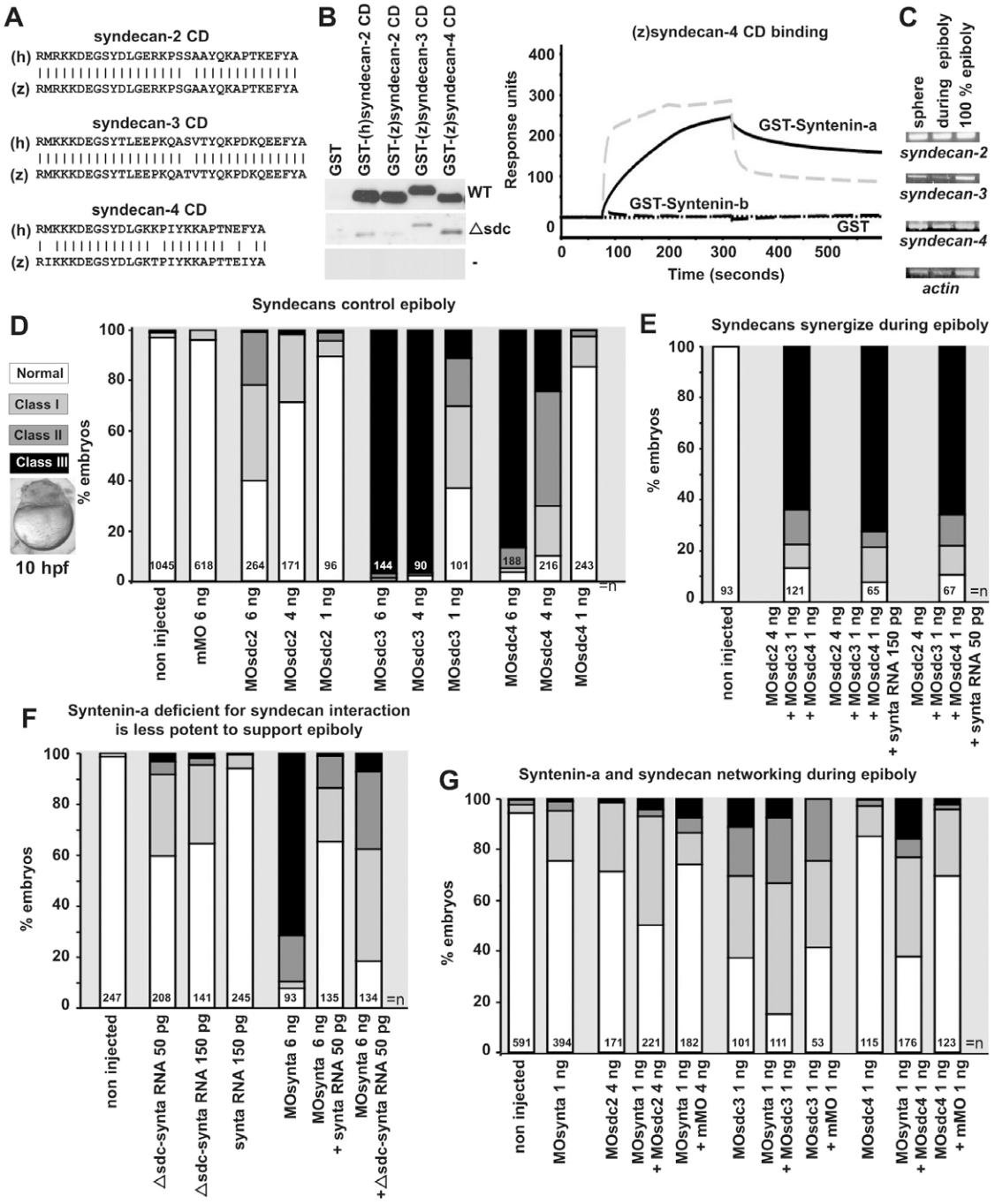

Fig. 5. Syndecans are important for epiboly initiation and progression. (**A**) Sequence alignments of the human (h) and zebrafish (z) syndecan cytoplasmic domains (CD). (**B**) Ligand-overlay experiments illustrating the binding of GST-myc-syntenin-a (WT, upper panel), GST-myc-syntenin-a mutated in the PDZ2 domain (Δsdc, middle panel) and GST–Myc (-, lower panel) to the different syndecan cytoplasmic domains (left). SPR experiments comparing the binding of syntenin-a (continuous black line) and syntenin-b (dashed black line) to the cytoplasmic domain of zebrafish syndecan-4 (right). The dashed grey line illustrates the binding of syntenin-b to the cytoplasmic domain of human syndecan-2 as positive control. Proteins were perfused at 1 μM. (**C**) RT-PCR illustrating the presence of RNA encoding syndecan-2, syndecan-3, syndecan-4 and actin at different stages. (**D**) Histogram illustrating the effects of morpholinos directed against the different syndecans (sdc). Analysis was done at 10 h.p.f. Class I and II defects are as in Fig. 1G. When morpholinos for sdc3 and sdc4 are used, class III contains many embryos blocked before 50% epiboly (micrograph), indicating these morpholinos induce epibolic defects at earlier stage than syntenin-a morpholino. (**E**) Histogram illustrating that morpholinos targeting different syndecans synergize to induce strong epibolic defects (compare with D) and the failure of RNA encoding syntenin-a to rescue those syndecan epibolic defects. (**F**) Histogram illustrating that the injection of RNA encoding a mutant syntenin-a with reduced syndecan interaction (Δsdc-synta) slightly affects epiboly in normal embryos and is less efficient at rescuing epiboly in morphants than RNA encoding wild-type syntenin-a. (**G**) Histogram showing that combined low doses of MOsynta and MOsdc, in particular MOscd4, are more effective in impairing epiboly than either MO alone. *n*, total number of embryos.

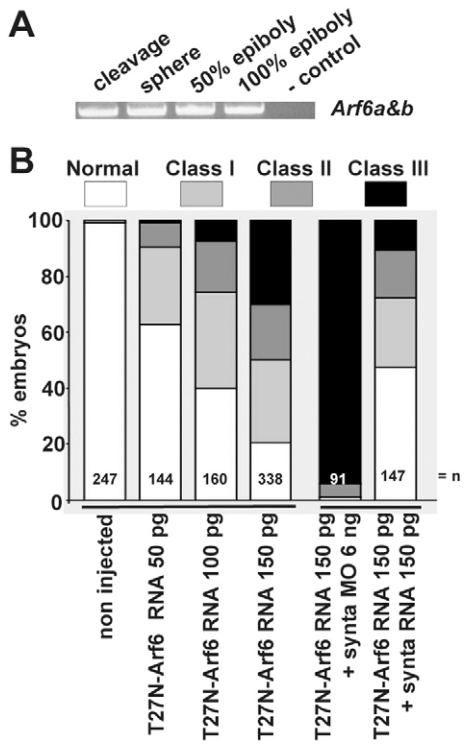

Fig. 6. Arf6 activity and the syntenin-a–Arf6 crosstalk are required for epiboly. (**A**) Expression of Arf6 RNA, as detected by RT-PCR at different stages. The primers amplify both cDNAs encoding Arf6. (**B**) Histogram illustrating the percentage of embryos found in each class (see Fig. 1G) when injecting increasing doses of RNA encoding dominant-negative T27N-Arf6, when injecting T27N-Arf6 RNA together with MOsynta or when co-injecting T27N-Arf6 RNA with synta RNA. Note that T27N-Arf6 synergizes with MOsynta to block epiboly, and that the effects of T27N-Arf6 are rescued by synta RNA. *n*, total number of embryos.

(data not shown). We therefore decided to test connections to Arf6 using a dominant-negative T27N mutant of Arf6-a (T27N-Arf6), which is defective in GTP-binding. The T27N-Arf6 inhibits the function of endogenous Arf6, which depends on its GTPase cycle, by sequestering Arf6-GEFs. The T27N-Arf6 mutant was shown to block the recycling of cell surface molecules, using the Arf6 endocytic route, back to the cell surface (Radhakrishna and Donaldson, 1997). Overexpression of T27N-Arf6 in zebrafish delayed epiboly progression in a concentration dependent manner. Of note, T27N-Arf6 effects on epiboly were similar to effects of synta morpholinos. Most severely affected embryos were blocked at 50% epiboly, but never earlier. Injection of 50 pg of T27N-Arf6 RNA induced epibolic defects in 37% of the embryos (n=144), with 1% displaying class III defects. Injection of 100 or 150 pg of T27N-Arf6 RNA gave 60% or 79% embryos, respectively (n=160 or n=338), with epibolic delay, with 8% or 30% displaying class III defects (Fig. 6B, left). Co-injection of 150 pg of T27N-Arf6 with 6 ng of MOsynta severely aggravated the defects, yielding 99% embryos (n=91) with epibolic defects and 93% class III. More importantly, co-injection of 50 pg of synta RNA (n=147) clearly rescued the T27N-Arf6 epibolic phenotype (Fig. 6B, right). These results indicate the networking of syntenin-a with Arf6 is crucial for epibolic progression.

The function of syntenin in cargo recycling from Arf6 endosomes strictly depends on its interaction with PIP2 in human cells in culture (Zimmermann et al., 2002; Zimmermann et al., 2005). This is explained by an Arf6-specific sorting mechanism where activated Arf6 recruits the PIP 5-kinase, which controls PIP2 biosynthesis on recycling endosomes (Donaldson, 2003). We therefore investigated a role for syntenin-a–PIP2 interaction in the control of epiboly movement.

We first confirmed that PIP2 interaction is conserved in zebrafish syntenin-a (Fig. 7A). We also verified the relevance of PIP2 binding for plasma membrane localization of syntenin in cells. Analogous to experiments performed for human syntenin (Zimmermann et al., 2002), we fused the tandem PDZs and the C-terminal domain of syntenin-a (P111-V299) to eYFP. In cells, the eYFP fluorescence of the P111-V299 construct was targeted to the plasma membrane and colocalized with eCFP fused to the PH domain of PLCδ, which is a probe for plasma membrane PIP2 (Varnai and Balla, 1998). Furthermore, eCFP and eYFP fluorescence simultaneously redistributed from the plasma membrane to the cytosol upon PIP2 breakdown induced by ionomycin and calcium (Fig. 7B). High-affinity binding of syntenin-a to PIP2 was abolished by introducing mutations in the PDZ1 domain (ΔPIP2–syntenin-a; see supplementary material Fig. S1A for the position and conservation of the residues). Equivalent mutations in human syntenin reduce PIP2 interaction by 95% (Zimmermann et al., 2002). As expected, surface plasmon resonance (SPR) experiments with GST–syntenin-a and GST–ΔPIP2–syntenin-a fusion proteins showed that PIP2 binding was strongly affected (Fig. 7A) and ΔPIP2–syntenin-a (Pro111-Val299) did not concentrate at the plasma membrane when overexpressed in cells as an eYFP fusion (Fig. 7C). The importance of PIP2 binding for epiboly was investigated by injecting RNA encoding ΔPIP2–syntenin-a (ΔPIP2–synta). Injection of 50 pg ΔPIP2–synta resulted in epibolic delay in 29% of the embryos (n=112), with 150 pg producing defects in 50% of the embryos (n=183). Injection of 150 pg RNA encoding wild-type syntenin-a yielded no more than 6% of embryos with epibolic delay (n=245) (Fig. 7E, left). Wild-type and mutant proteins were synthesized at similar levels (Fig. 7D). This indicates that ΔPIP_2–syntenin-a acts as a dominant-negative on epiboly progression. In addition, unlike RNA encoding wild-type syntenin-a (n=224), ΔPIP2–synta (n=251) was not able to correct epibolic defects caused by the depletion of syntenin-a (Fig. 7E, right). Thus, the function of syntenin-a during epiboly appears to be strictly dependent on the interaction with PIP2.

Discussion

In this study, we investigated the in vivo function of the syntenin PDZ complex and highlight a novel molecular pathway controlling gastrulation movements in zebrafish. We found two syntenins for which mRNA were present maternally. Knockdown of syntenin-a impaired the progression of epiboly of all layers (YSL, deep cells, EVL) beyond 50% and also impaired convergent extension of the deep cells. Morpholinos affecting syntenin-b translation or syntenin-a splicing had no such effects on epiboly, but also clearly compromised early development and convergent extension movements (data not shown). Focusing on syntenin-a morphants, we observed no primary problems in cell fate specification, division or viability, but rather identified syntenin-a as a regulator of embryonic cell movement. However,

syntenin-a does not appear to act as a general motility factor. Indeed, the initial phases of epiboly and mesoderm internalization (germ ring) are unaffected in morphants. Depletion of syntenin-a in the whole embryo blocks epiboly and impairs body-axis formation, whereas depleting syntenin-a solely in the YSL also blocks epiboly, but results in embryos with a well-formed axis. This observation supports the view that epiboly and gastrulation movements (convergent extension), are independent processes (Strahle and Jesuthasan, 1993). In vertebrates, the convergent extension process is governed by the non-canonical Wnt signaling pathway (Roszko et al., 2009). Interestingly, Luyten and co-workers (Luyten et al., 2008) showed that syntenin interacts with the Wnt receptor protein Frizzled-7 and supports non-canonical Wnt signaling, in particular the PKCα and CDC42 branch in *Xenopus* animal cap assays. Moreover, a pool of morpholinos directed against the three syntenin forms present in *Xenopus* reduces elongation of the body axis (Luyten et al., 2008). By comparison, the morphant phenotype observed in zebrafish manifests itself earlier, is more drastic and is observed upon depletion of solely the syntenin-a form.

By analyzing the epibolic phenotype, we established that syntenin-a controls the autonomous vegetal expansion of the YSL, an essential pulling force for epiboly progression. We addressed the effect of syntenin-a on various fundamental mechanisms of this process that have been proposed and found anomalies of the actin cytoskeleton. Normally by 50% epiboly, a punctate band of actin and myosin forms within the eYSL close to the interface between the eYSL and the EVL margin that, together with the EVL cellular rearrangements, is thought to function as a purse-string pulling the YSL and EVL towards the vegetal pole (Cheng et al., 2004; Zalik et al., 1999). This punctate band is broadened in syntenin-a morphants, but constriction still occurs, as shown by the constriction of embryos at the equator at 10 h.p.f. This suggests that the contractile forces are preserved, but that YSL has lost its property to move and pull vegetally, which is consistent with the 'roundness' of the EVL cells. The EVL cells of syntenin-a morphants display a disturbed cortical actin, with ruffling activity. Although intrinsic abnormal cortical actin dynamics in the EVL might contribute to impaired epiboly progression (Koppen et al., 2006), the ruffling activity in the EVL might just come as a consequence of the loss of vegetal expansion as a result of the lack of progression of the YSL and tension.

We also studied molecular players underlying the control of epiboly progression by syntenin-a. We propose that they comprise Arf6, PIP2 and possibly syndecan-4. The small GTPase Arf6 is involved in various aspects of cell adhesion and migration. The mechanisms are diverse and involve effects on the lipid microenvironment, vesicular transport and direct regulation of Rho-family GTPase function (D′Souza-Schorey and Chavrier, 2006; Myers and Casanova, 2008). Overexpression of a constitutive inactive Arf6 induces epibolic defects similar to those of syntenin-a morphants and the two molecules genetically

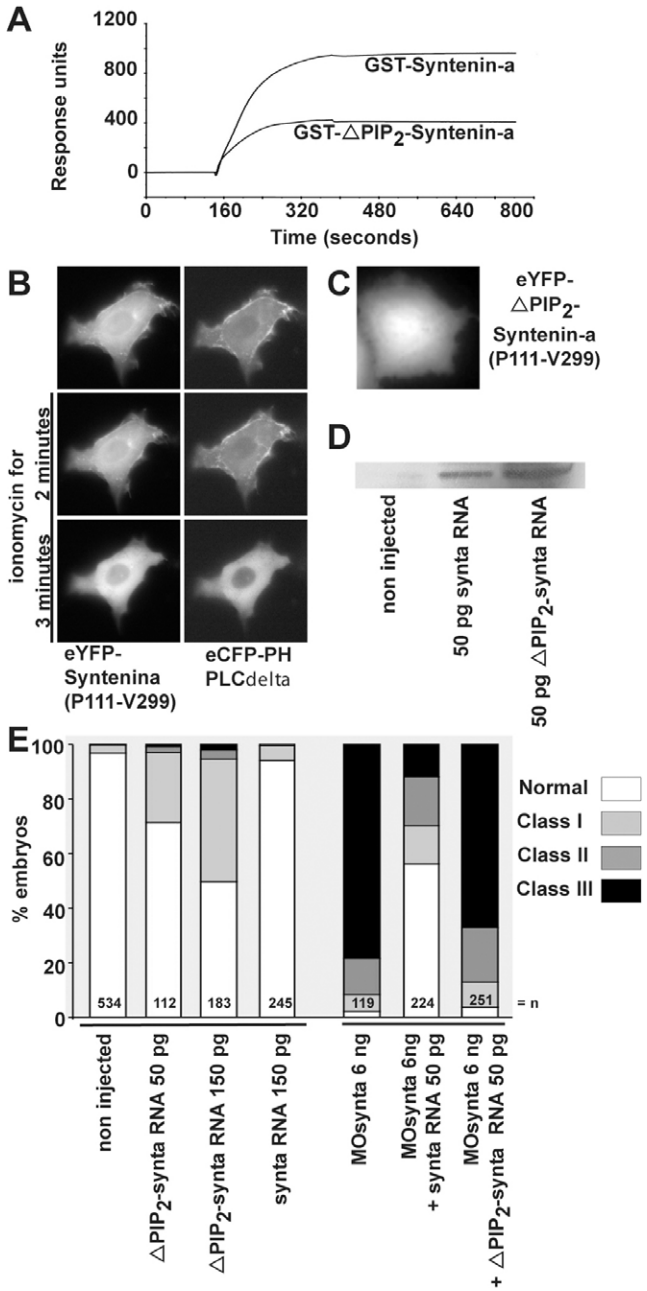

Fig. 7. Syntenin-a interaction with PIP2 is required for epiboly progression. (**A**) SPR experiment showing the binding of syntenin-a, and the reduced binding of the syntenin-a PDZ1 mutant (ΔPIP2–syntenin-a), to PIP2-containing liposomes. Proteins were perfused at 0.5 μM. (**B**) Time-lapse microscopy of a MCF-7 cell, before and after ionomycin-induced plasma membrane PIP2 breakdown. The cell overexpressed the PDZ tandem and C-terminal domain of syntenin-a (P111-V299) fused to eYFP, and the PH domain of PLCδ fused to eCFP. Syntenin-a (P111-V299) colocalizes with PH-PLCδ, and both fluorescent signals delocalize simultaneously from the plasma membrane after PIP2 breakdown, indicative of a syntenin-a–PIP2 interaction in a cellular context. (**C**) Micrograph of a MCF-7 cell expressing syntenin-a (Pro111-Val299) with a mutant PDZ1 domain deficient for PIP2 binding, fused to eYFP, showing no plasma membrane enrichment. (**D**) Western blot showing that injection of 50 pg of RNA encoding either wild-type or ΔPIP2–syntenin-a yields similar levels of protein expression. (**E**) Left part, percentage of embryos found in each class (as in Fig. 1G) upon injection of RNA encoding syntenin-a deficient for PIP2 interaction (ΔPIP_2-synta) or wild-type syntenin-a (synta). Right bars show percentage of embryos found in each class upon injection of MOsynta, together with wild-type or ΔPIP_2–syntax. Note that ΔPIP_2-synta expression affects epiboly by itself, and has no rescue potential.

interact. Moreover, syntenin-a overexpression rescues the epiboly defects observed with inactive Arf6. In cultured mammalian cells, syntenin is a rate-limiting factor for Arf6-dependent recycling. Syntenin supports the recycling of its PDZ ligand syndecan (and most probably other PDZ target receptors) by its ability to directly bind PIP2, the product of the Arf6 effector PIP 5-kinase (Honda et al., 1999). Syntenin-a deficient in PIP2 interaction impairs epiboly progression and is unable to rescue the effects of syntenin-a morpholinos, strongly indicative of a role for syntenin-a, PIP2 and Arf6 recycling in the progression of epiboly. Unfortunately, recycling has not so far been reported in zebrafish YSL and we could not observe it in our microscopic setting. Injection of RNA encoding Arf6–eGFP failed to highlight vesicles: the fluorescence was weak and mainly diffuse.

Among the numerous transmembrane receptors and other molecules binding to syntenin and susceptible to recycling in a syntenin-Arf6-dependent manner, none has been reported to function in zebrafish epiboly, although most of them are expressed at this stage. Syndecans, because of their relative abundance, are probably the preferential partners of syntenin (Grootjans et al., 2000) and their expression and role during zebrafish epiboly was unknown. We found that all zebrafish syndecans (2, 3 and 4) are expressed maternally and that their depletion impairs epiboly. Syndecan-2 has mild effects on epiboly progression, whereas depletion of syndecan-3 or syndecan-4 blocks the initiation of epiboly, thus these two proteins act slightly earlier than syntenin-a and Arf6. The syndecan-3 and syndecan-4 morphants resemble embryos treated with the chemical FGF receptor inhibitor SU5402, and ERK2 morphants, which also fail to initiate epiboly (Krens et al., 2008), and this might be due to the crucial role of syndecans in FGF signaling (Steinfeld et al., 1996). We do not observe a block of epiboly initiation in syntenin morphants, even when combining morpholinos directed against *syntenin-a* and *syntenin-b* (not shown). Assuming that a role for traces of maternal proteins can be excluded, this indicates that syntenin is not required for early aspects of syndecan function. However, morpholinos against syndecan-4 appear to synergize with syntenin-a morpholinos to block epiboly, suggesting that signaling pathways specifically controlled by syndecan-4 might be implicated in the syntenin-a epiboly defects. This appears to be consistent with the observation that syntenin-b, which does not bind syndecan-4 (supplementary material Fig. S4A) is not required for epiboly (not shown). Syndecan-4 was shown to determine directional migration by controlling the local activity of the actin regulator Rac in response to fibronectin (Bass et al., 2007; Matthews et al., 2008). It has been proposed that the pool of active Rac at the plasma membrane relies on Arf6-mediated recycling of endosome-associated Rac (reviewed by Myers and Casanova, 2008). Because Leskow and colleagues (Leskow et al., 2006) reported that downregulation of the Rac-GAP chimerin, increasing Rac activity, slightly accelerates epiboly (Leskow et al., 2006), we also tested for genetic interaction between syntenin-a and chimerin in epiboly, but we could not validate a link between the two molecules (data not shown). We also exclude a role for fibronectin because we could not detect it at 50% epiboly, consistent with a recent report that fibronectin is first detected at the epiblast–hypoblast and blastoderm–yolk interface at 65% epiboly (Latimer and Jessen, 2010), thus later than the epiboly defects observed in syntenin-a morphants. In conclusion, our study describes novel steps in the molecular elucidation of the first cell movements in the early fish embryo by identifying the importance of the syntenin–syndecan–PIP2–Arf6 pathway for the progression of epiboly.

Materials and Methods

Cloning of zebrafish syntenins, syndecans and Arf6

Syntenin cDNAs were obtained from the IMAGE Consortium (Livermore, CA). *Syntenin-a* and *syntenin-b* correspond to the sequences deposited in the GenBank database under the accession number BC044454.1 and NM214798.1, respectively. The cDNA encoding zebrafish syndecan-3 was reconstituted in silico by iterative blasting of multiple EST databases. We cloned the corresponding ORF from a self-made cDNA library originating from bud stage total RNA extracts, and submitted the sequence (GenBank accession number HQ827172). Blasting the zebrafish genomic database with the cDNA sequence of human Arf6 provided the sequences for *Arf6-a* (NW001512173.1) and *Arf6-b* (NW001511633.1). DNAs encoding zebrafish syndecan-2, syndecan-3 and syndecan-4 and zebrafish *Arf6-a* and *Arf6-b* were isolated from our cDNA library by PCR.

Molecular biology

GST fusion constructs were obtained by cloning appropriate PCR fragments in the pGEX-5X vector (Amersham Pharmacia Biotech, Uppsala, Sweden). GST-fusion proteins were purified on Glutathione Sepharose 4B beads (Amersham Pharmacia Biotech). For fluorescent fusion constructs, the PCR fragments were cloned in mammalian expression vectors encoding *Aequorea victoria* fluorescent protein (Clontech, Palo Alto, CA). Morpholino oligonucleotides directed against the translational start sites, with the sequences 5′-TACAACGACATCCTTTCTGC-TTTCA-3′ (MOsynta), 5′-AACAAGCGACTTCTGAAGAAATGGG-3′ (MOsyntabis), 5′-TAgAACGAgATCgTTTgTGgTTTCA-3′ (misMOsynta), 5′-AAgAAcCGACT-TgTGAAcAAATcGG-3′ (misMOsyntabis), 5′-TTCCTCAGTCTTCGCTCGTGA-AAGC-3′ (MOsdc2), 5′-CTCCTCTTTCGGGTGGGTGTGA-3′ (MOsdc3), 5′-TGAGGTAAACTTTCAACATCTTCTC-3′ (MOsdc4), 5′-TTgCTgAGTCTTCcC-TCGTcAAAcC-3′ (mMOsdc2), 5′-cgcacaagtttaatcagtcggccta-3′ (control MO for sdc3), 5′-gagaagatgttgaaagtttacctca-3′ (control MO for sdc4), 5′-GATCTTG-GAAAGCATCTTCCCCATG-3′ (MOArf6-a), 5′-CTTTGACAGCATCTTCCC-CATCTTG-3′ (MOArf6-b) were obtained from Gene Tools LLC (Philomath, OR) or Openbiosystems (Huntsville, AL).

In vitro transcription–translation reactions were carried out using the TNT Quick Coupled Transcription/Translation System (Promega, Madison, WI). Reactions were performed in the presence of [^{35}S] methionine (15 µCi/mmol; Perkin Elmer) according to the recommendations of the manufacturer. The reaction products were analyzed by SDS-PAGE. After migration, the gel was fixed for 20 minutes in an aqueous solution containing 10% acetic acid and 10% methanol. The gel was dried for 1 hour and put in contact with a film for autoradiography. Probes for WISH were synthesized from cDNA using a DIG RNA labeling kit (Roche, Basel, Switzerland). Constructs for RNA injection in zebrafish were cloned in the pCS2+ vector, and capped mRNA was synthesized from linearized templates using the mMessage Machine Kit (Ambion, Austin, TX). DNAs with silent mutations not targeted by the morpholino, encoding full-length wild-type syntenin-a, syntenin deficient for syndecan or PIP2 binding and T27N Arf6-a, respectively, were obtained by site-directed mutagenesis.

RNA isolation, cDNA synthesis, RT-PCR and western blotting

Embryos of the desired developmental stage were collected and homogenized in Trizol (Life Technologies, Grand Island, NY). RNA was purified by chloroform extraction, followed by isopropanol precipitation. cDNA was synthesized by reverse transcription of 5 µg of total RNA, using Superscript III Reverse Transcriptase and random hexamer primers (Invitrogen, Carlsbad, CA). Detection of RNA transcripts was by standard PCR, using reverse-transcribed RNA as template. Primers were designed to amplify complete coding sequences, spanning different introns in genomic DNA. For western blotting, proteins were extracted from 10 h.p.f. embryos, resuspended loading buffer, fractionated by SDS-PAGE and transferred to a nitrocellulose membrane (Hybond C extra, Amersham Biosciences, Amersham, UK). After blocking, the membrane was incubated at room temperature with 1 µg/µl Ab96 and with goat-anti rabbit antibody conjugated to horseradish peroxidise (HRP) before signals were detected by enhanced chemiluminescence (ECL; Perkin Elmer, Waltham, MA).

Ligand-overlay experiments

GST and GST fusion proteins (2 µg), fractionated by 10% SDS-PAGE and transferred to nitrocellulose membranes, were incubated overnight with 10 µg/ml of GST–Myc constructs at 4°C. Binding was detected by incubation with an antibody against Myc (Santa Cruz Biotechnology, Santa Cruz, CA, clone 9E10), HRP-coupled secondary antibody (Amersham Biosciences, Amersham, UK) and ECL.

Surface plasmon resonance experiments

SPR experiments were performed as described previously (Koo et al., 2006; Mortier et al., 2005). For syndecan-binding experiments, 300 response units of N-terminally biotinylated synthetic peptide were immobilized onto a streptavidin sensor chip (Biacore Life Sciences, Uppsala, Sweden). For PIP2 binding experiments, L1 chips (Biacore Life Sciences) were coated with reconstituted liposomes containing phosphatidylcholine, phosphatidylethanolamine, phosphatidylserine (Sigma) and either phosphatidylinositol or PIP_2 (Avanti Polar Lipids, Alabaster, AL) in the molar ratios 3:4:2:1. GST-fusion proteins were perfused over coated chips at a flow rate of 30 µl/minutes. For PIP2 binding, the sensorgrams were corrected for background association to composite vesicles containing 10% phosphatidylinositol. Experiments were performed using a Biacore 2000 or T100 instrument (Pharmacia Biosensor or GE Healthcare, Uppsala, Sweden).

Membrane recruitment experiments

MCF-7 cells (American Type Culture Collection, Manassas, VA) were grown in DMEM/F12 medium (Life Technologies, Grand Island, NY) plus 10% fetal bovine serum (Hyclone, South Logan, UT). Cells were plated on chamber slides (Nalge Nunc, Rochester, NY) and transfected using FuGENE 6 (Roche, Basel, Switzerland). Plasma membrane PIP2 breakdown experiments were as described earlier (Varnai and Balla, 1998). Time-lapse microscopy was performed with the Leica AS MDW workstation (Leica Microsystems, Wetzlar, Germany).

Injections in zebrafish

AB wild-type zebrafish (*Danio rerio*; Hamilton strain) embryos were kept at 28.5℃, manipulated in E3 embryo medium and staged according morphology and time after fertilization (Kimmel et al., 1995). Morpholinos were dissolved in Danieau buffer. For injection, morpholinos and RNAs were diluted in Danieau buffer containing 25 µg/ml of fluorescently labelled dextran (Molecular Probes, Eugene, OR). Solely embryos with homogenous fluorescence were considered. Sytox Green (Molecular Probes) was injected at 25 µM (D′Amico and Cooper, 2001).

Staining and imaging of zebrafish embryos

When needed, embryos were dechorionated manually. WISH was performed as described earlier (Jowett, 2001). Probes corresponded to full-length open reading frames. Staining of microtubules and actin was performed as previously described (Koppen et al., 2006; Solnica-Krezel and Driever, 1994). Microscopic analyses were performed with a Leica Fluo Combi stereomicroscope connected to a Leica DC300 F camera (Leica Microsystems, Wetzlar, Germany). Confocal microscopy was performed with a Bio-Rad MRC-1024 Laser Scanning Confocal Imaging System (Carl Zeiss Microimaging, Thornwood, NY) or an Olympus Fluo View 1000 (Olympus, Center Valley, PA). Quantitative Acridine Orange assays were performed as described earlier (Detrich et al., 2004). Embryos used as positive controls were incubated for 3 hours with 100 µg/ml of cycloheximide, before staining with Acridine Orange (Sigma). Fluorescence was measured with a FluoStar Galaxy microplate reader (BMG Labtechnologies, Offenburg, Germany). For immunohistochemistry, anti-syntenin antibodies (Ab96) were purified from the serum of a rabbit immunized with a peptide (PSIMKSLMDHTIPEV) corresponding to part of the C-terminal domain of mouse syntenin (Eurogentec, Seraing, Belgium). Their cross-reaction with both zebrafish syntenins was established in western blot. They were validated for immunohistochemistry on mouse sections by competition experiments with recombinant syntenin. zebrafish embryos were fixed for 3 hours in 4% paraformaldehyde. After blocking for 2 hours in PBS containing 0.5% Triton X-100, 1% BSA and 2% fetal calf serum, the embryos were incubated overnight with (0.5 µg/ml) Ab96 or antibodies against phosphorylated histone H3 antibody (1:100) (Cell Signaling). Colour reaction was developed using HRP-conjugated secondary antibodies and diaminobenzidine solution (Sigma). Images were collected using a Leica compound microscope (Leica Microsystems, Wetzlar, Germany) connected to a SPOT camera (Visitron Systems, Puchheim, Germany).

Transmission electron microscopy

Fish injected with 6 ng of misMOsynta or MOsynta and collected at 6 h.p.f. were fixed for 2 hours at 24℃ with 3% glutaraldehyde in 0.1 M sodium cacodylate. After overnight washing with 0.1 M sodium cacodylate, embryos were post-fixed with 1% osmium tetroxide in 0.1 M phosphate buffer for 1 hour at 24℃, washed with 0.1 M phosphate buffer, dehydrated in a graded series of ethanol and finally embedded in Agar 100. Ultrathin sections were stained with uranyl acetate and lead citrate and viewed with a JEOL-JEM2100 microscope.

Acknowledgements

We thank Danny Huylebroeck, the Cell Imaging Core, K. U. Leuven, the EM facility at CME-VIB K. U. Leuven and the Zebrafish International Resource Center for feedback, services and materials. The zebrafish International Resource Center is supported by the National Institutes of Health (NCRR) [grant number P40 RR12546].

Funding

This work was supported by the Interuniversity Attraction Poles of the Prime Ministers Services (IAP, phase VI); the Fund for Scientific Research-Flanders (FWO); the Concerted Actions Program, K. U. Leuven; the Belgian Federation against Cancer; and EMBO YIP. Y.I. is the recipient of an EMBO long-term fellowship.

Supplementary material available online at
http://jcs.biologists.org/lookup/suppl/doi:10.1242/jcs.089987/-/DC1

References

Bass, M. D., Roach, K. A., Morgan, M. R., Mostafavi-Pour, Z., Schoen, T., Muramatsu, T., Mayer, U., Ballestrem, C., Spatz, J. P. and Humphries, M. J. (2007). Syndecan-4-dependent Rac1 regulation determines directional migration in response to the extracellular matrix. *J. Cell Biol.* **177**, 527-538.

Beekman, J. M. and Coffer, P. J. (2008). The ins and outs of syntenin, a multifunctional intracellular adaptor protein. *J. Cell Sci.* **121**, 1349-1355.

Betchaku, T. A. T. J. (1986). Programmed endocytosis during epiboly of Fundulus heteroclitus. *Amer. Zool* **26**, 193-196.

Carvalho, L. and Heisenberg, C. P. (2010). The yolk syncytial layer in early zebrafish development. *Trends Cell Biol.* **10**, 586-592.

Chen, E., Hermanson, S. and Ekker, S. C. (2004). Syndecan-2 is essential for angiogenic sprouting during zebrafish development. *Blood* **103**, 1710-1719.

Cheng, J. C., Miller, A. L. and Webb, S. E. (2004). Organization and function of microfilaments during late epiboly in zebrafish embryos. *Dev. Dyn.* **231**, 313-323.

D'Amico, L. A. and Cooper, M. S. (2001). Morphogenetic domains in the yolk syncytial layer of axiating zebrafish embryos. *Dev. Dyn.* **222**, 611-624.

D'Souza-Schorey, C. and Chavrier, P. (2006). ARF proteins: roles in membrane traffic and beyond. *Nat. Rev. Mol. Cell Biol.* **7**, 347-358.

Detrich, H. W., Westerfield, M. and Zon, L. I. (2004). The Zebrafish: Cellular and Developmental Biology (Second Edition). Elsevier Academic Press, Amsterdam.

Donaldson, J. G. (2003). Multiple roles for Arf6: sorting, structuring, and signaling at the plasma membrane. *J. Biol. Chem.* **278**, 41573-41576.

Grootjans, J. J., Zimmermann, P., Reekmans, G., Smets, A., Degeest, G., Durr, J. and David, G. (1997). Syntenin, a PDZ protein that binds syndecan cytoplasmic domains. *Proc. Natl. Acad. Sci. USA* **94**, 13683-13688.

Grootjans, J. J., Reekmans, G., Ceulemans, H. and David, G. (2000). Syntenin-syndecan binding requires syndecan-synteny and the co-operation of both PDZ domains of syntenin. *J. Biol. Chem.* **275**, 19933-19941.

Honda, A., Nogami, M., Yokozeki, T., Yamazaki, M., Nakamura, H., Watanabe, H., Kawamoto, K., Nakayama, K., Morris, A. J., Frohman, M. A. et al. (1999). Phosphatidylinositol 4-phosphate 5-kinase alpha is a downstream effector of the small G protein ARF6 in membrane ruffle formation. *Cell* **99**, 521-532.

Jowett, T. (2001). Double in situ hybridization techniques in zebrafish. *Methods* **23**, 345-358.

Kimmel, C. B., Ballard, W. W., Kimmel, S. R., Ullmann, B. and Schilling, T. F. (1995). Stages of embryonic development of the zebrafish. *Dev. Dyn.* **203**, 253-310.

Koo, B. K., Jung, Y. S., Shin, J., Han, I., Mortier, E., Zimmermann, P., Whiteford, J. R., Couchman, J. R., Oh, E. S. and Lee, W. (2006). Structural basis of syndecan-4 phosphorylation as a molecular switch to regulate signaling. *J. Mol. Biol.* **355**, 651-663.

Koppen, M., Fernandez, B. G., Carvalho, L., Jacinto, A. and Heisenberg, C. P. (2006). Coordinated cell-shape changes control epithelial movement in zebrafish and Drosophila. *Development* **133**, 2671-2681.

Krens, S. F., He, S., Lamers, G. E., Meijer, A. H., Bakkers, J., Schmidt, T., Spaink, H. P. and Snaar-Jagalska, B. E. (2008). Distinct functions for ERK1 and ERK2 in cell migration processes during zebrafish gastrulation. *Dev. Biol.* **319**, 370-383.

Lachnit, M., Kur, E. and Driever, W. (2008). Alterations of the cytoskeleton in all three embryonic lineages contribute to the epiboly defect of Pou5f1/Oct4 deficient MZspg zebrafish embryos. *Dev. Biol.* **315**, 1-17.

Lambaerts, K., Wilcox-Adelman, S. A. and Zimmermann, P. (2009). The signaling mechanisms of syndecan heparan sulfate proteoglycans. *Curr. Opin. Cell Biol.* **21**, 662-669.

Latimer, A. and Jessen, J. R. (2010). Extracellular matrix assembly and organization during zebrafish gastrulation. *Matrix Biol.* **29**, 89-96.

Lepage, S. E. and Bruce, A. E. (2010). Zebrafish epiboly: mechanics and mechanisms. *Int. J. Dev. Biol.* **54**, 1213-1228.

Leptin, M. (2005). Gastrulation movements: the logic and the nuts and bolts. *Dev. Cell* **8**, 305-320.

Leskow, F. C., Holloway, B. A., Wang, H., Mullins, M. C. and Kazanietz, M. G. (2006). The zebrafish homologue of mammalian chimerin Rac-GAPs is implicated in epiboly progression during development. *Proc. Natl. Acad. Sci. USA* **103**, 5373-5378.

Luyten, A., Mortier, E., Van Campenhout, C., Taelman, V., Degeest, G., Wuytens, G., Lambaerts, K., David, G., Bellefroid, E. J. and Zimmermann, P. (2008). The postsynaptic density 95/disc-large/zona occludens protein syntenin directly interacts with frizzled 7 and supports noncanonical Wnt signaling. *Mol. Biol. Cell* **19**, 1594-1604.

Matthews, H. K., Marchant, L., Carmona-Fontaine, C., Kuriyama, S., Larrain, J., Holt, M. R., Parsons, M. and Mayor, R. (2008). Directional migration of neural

crest cells in vivo is regulated by Syndecan-4/Rac1 and non-canonical Wnt signaling/RhoA. *Development* **135**, 1771-1780.

Mortier, E., Wuytens, G., Leenaerts, I., Hannes, F., Heung, M. Y., Degeest, G., David, G. and Zimmermann, P. (2005). Nuclear speckles and nucleoli targeting by PIP2-PDZ domain interactions. *EMBO J.* **24**, 2556-2565.

Myers, K. R. and Casanova, J. E. (2008). Regulation of actin cytoskeleton dynamics by Arf-family GTPases. *Trends Cell Biol.* **18**, 184-192.

Nourry, C., Grant, S. G. and Borg, J. P. (2003). PDZ domain proteins: plug and play! *Sci. STKE* **2003**, RE7.

Radhakrishna, H. and Donaldson, J. G. (1997). ADP-ribosylation factor 6 regulates a novel plasma membrane recycling pathway. *J. Cell Biol.* **139**, 49-61.

Rohde, L. A. and Heisenberg, C. P. (2007). Zebrafish gastrulation: cell movements, signals, and mechanisms. *Int. Rev. Cytol.* **261**, 159-192.

Roszko, I., Sawada, A. and Solnica-Krezel, L. (2009). Regulation of convergence and extension movements during vertebrate gastrulation by the Wnt/PCP pathway. *Semin. Cell Dev. Biol.* **20**, 986-997.

Solnica-Krezel, L. (2005). Conserved patterns of cell movements during vertebrate gastrulation. *Curr. Biol.* **15**, R213-R228.

Solnica-Krezel, L. (2006). Gastrulation in zebrafish – all just about adhesion? *Curr. Opin. Genet Dev.* **16**, 433-441.

Solnica-Krezel, L. and Driever, W. (1994). Microtubule arrays of the zebrafish yolk cell: organization and function during epiboly. *Development* **120**, 2443-2455.

Steinfeld, R., Van Den Berghe, H. and David, G. (1996). Stimulation of fibroblast growth factor receptor-1 occupancy and signaling by cell surface-associated syndecans and glypican. *J. Cell Biol.* **133**, 405-416.

Strahle, U. and Jesuthasan, S. (1993). Ultraviolet irradiation impairs epiboly in zebrafish embryos: evidence for a microtubule-dependent mechanism of epiboly. *Development* **119**, 909-919.

Trinkaus, J. P. (1951). A study of the mechanisms of epiboly in the egg of fundulus heteroclitus. *J. Exp. Zool.* **118**, 269-319.

Varnai, P. and Balla, T. (1998). Visualization of phosphoinositides that bind pleckstrin homology domains: calcium- and agonist-induced dynamic changes and relationship to myo-[3H]inositol-labeled phosphoinositide pools. *J. Cell Biol.* **143**, 501-510.

Warga, R. M. and Kimmel, C. B. (1990). Cell movements during epiboly and gastrulation in zebrafish. *Development* **108**, 569-580.

Whiteford, J. R. and Couchman, J. R. (2006). A conserved NXIP motif is required for cell adhesion properties of the syndecan-4 ectodomain. *J. Biol. Chem.* **281**, 32156-32163.

Zalik, S. E., Lewandowski, E., Kam, Z. and Geiger, B. (1999). Cell adhesion and the actin cytoskeleton of the enveloping layer in the zebrafish embryo during epiboly. *Biochem. Cell Biol.* **77**, 527-542.

Zimmermann, P., Meerschaert, K., Reekmans, G., Leenaerts, I., Small, J. V., Vandekerckhove, J., David, G. and Gettemans, J. (2002). PIP(2)-PDZ domain binding controls the association of syntenin with the plasma membrane. *Mol. Cell* **9**, 1215-1225.

Zimmermann, P., Zhang, Z., Degeest, G., Mortier, E., Leenaerts, I., Coomans, C., Schulz, J., N'Kuli, F., Courtoy, P. J. and David, G. (2005). Syndecan recycling [corrected] is controlled by syntenin-PIP2 interaction and Arf6. *Dev. Cell* **9**, 377-388.

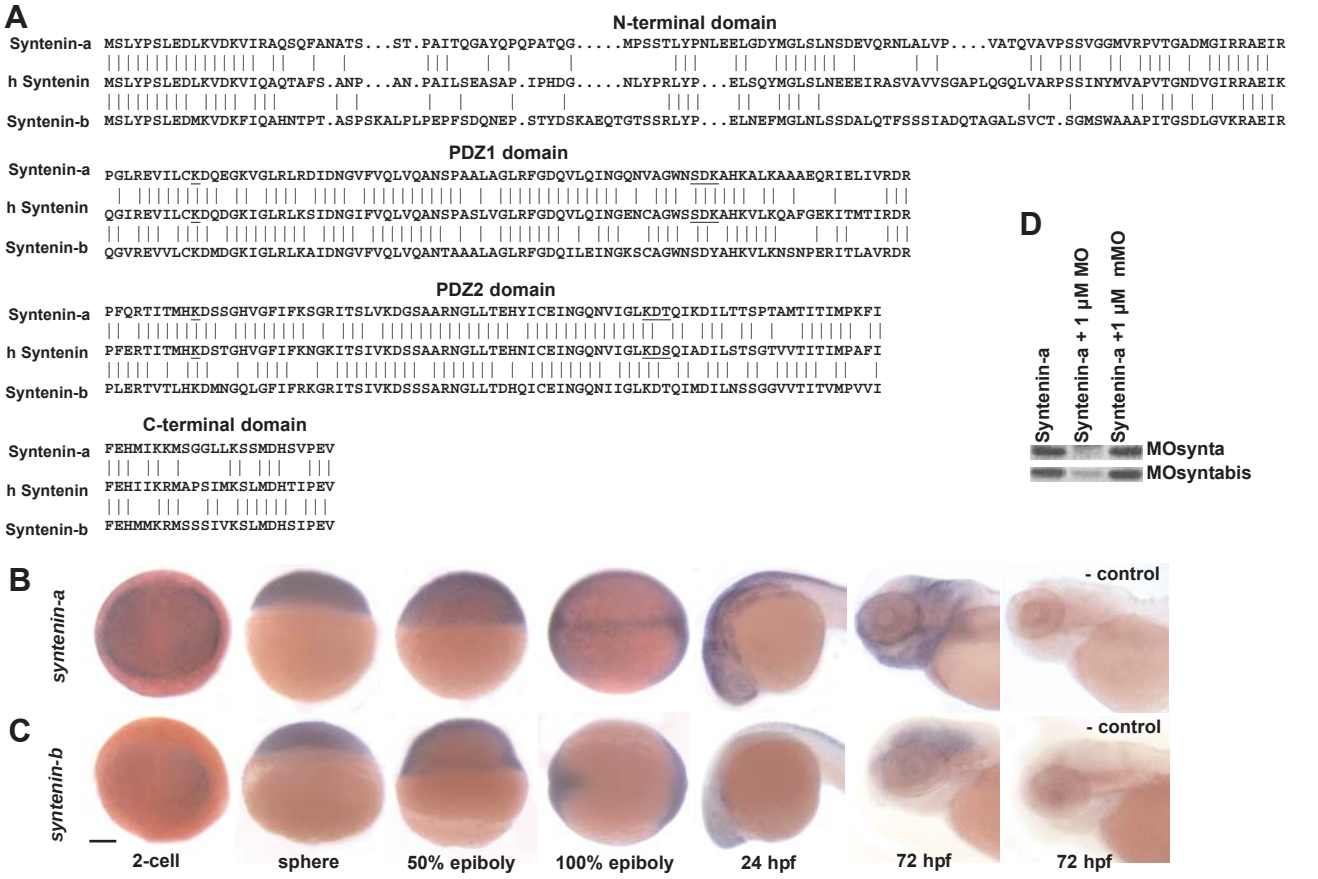

Fig. S1 Syntenin-a and -b in zebrafish, developmental expressions and effectiveness of morpholinos. (A) Sequence alignment of the two zebrafish Syntenins with human (h) Syntenin. Both proteins have similar domain organizations as the Syntenins found in other organisms, namely an N-terminal region, two PDZ domains in tandem and a C-terminal domain. Syntenin-a and Syntenin-b are 61% identical and, respectively, 69% and 61% similar to human Syntenin. The PDZ tandem, mediating most of the Syntenin interactions described so far, is highly conserved compared to the N-terminal region and the C-terminal domain. Underlined residues in the PDZ1 domain correspond to residues mutated for the PIP_2-interaction studies, Ala substituting for Lys120 and His-Glu-Gln replacing the residues 172Ser-Asp-Lys174. Underlined residues in the PDZ2 domain correspond to residues mutated for the syndecan-interaction studies, Ala substituting for Lys204 and Ser-His-Glu replacing the residues 251Lys-Asp-Thr253. (B,C) WISH illustrating the spatio-temporal expression of *syntenin-a* (B) and *syntenin-b* (C) transcripts at different stages of embryonic development, as indicated. Images correspond to lateral views except for the 2-cell stages which are animal pole views and the 100% epiboly stages which are dorsal views. The specificity of the reaction is illustrated for 72 hours post fertilization (hpf) embryos, showing no staining when a sense probe is used. Note that by 24 hpf, both signals became more restricted to the nervous systems. By 72 hpf, the Syntenin transcripts distributed in different brain areas. (D) Syntenin-a morpholinos, MOsynta and MOsyntabis, designed to inhibit the translation of *syntenin-a* mRNA are effective, as tested by in vitro transcription-translation assays, while their mismatch derivatives (mMO) have no effect on this translation.

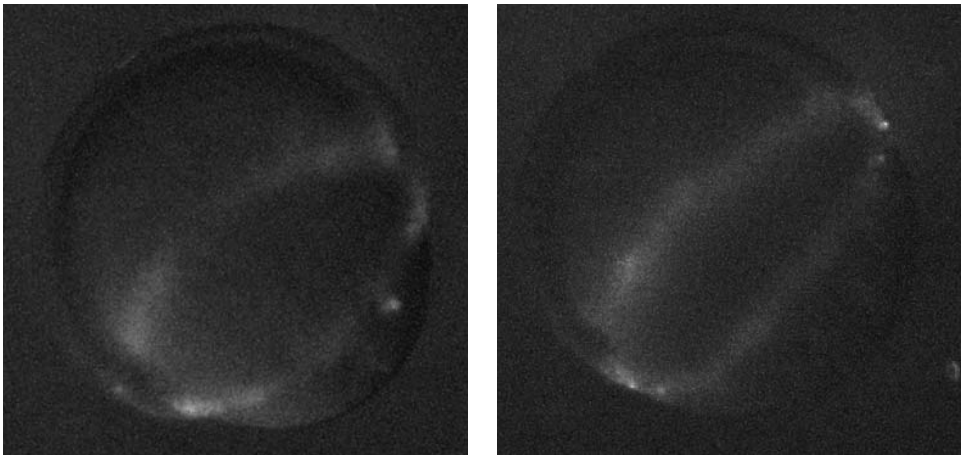

Fig. S2. The process of YSL endocytosis is not disrupted in Syntenin-a morphants. Views of embryos at 6.7 hpf incubated with Rhodamine-dextran showing the endocytic ring in control (left) and in 6 ng syntaMO-injected (right) embryos. To label endocytic vesicles, embryos at shield stage were placed in a 10 mg/ml solution of Rhodamine-labeled dextran (10.000 MW, Molecular probes). After 30 min of loading, embryos were washed and analysed immediately. Microscopic analyses were performed with a Leica Fluo Combi stereomicroscope connected to a Leica DC300 F camera.

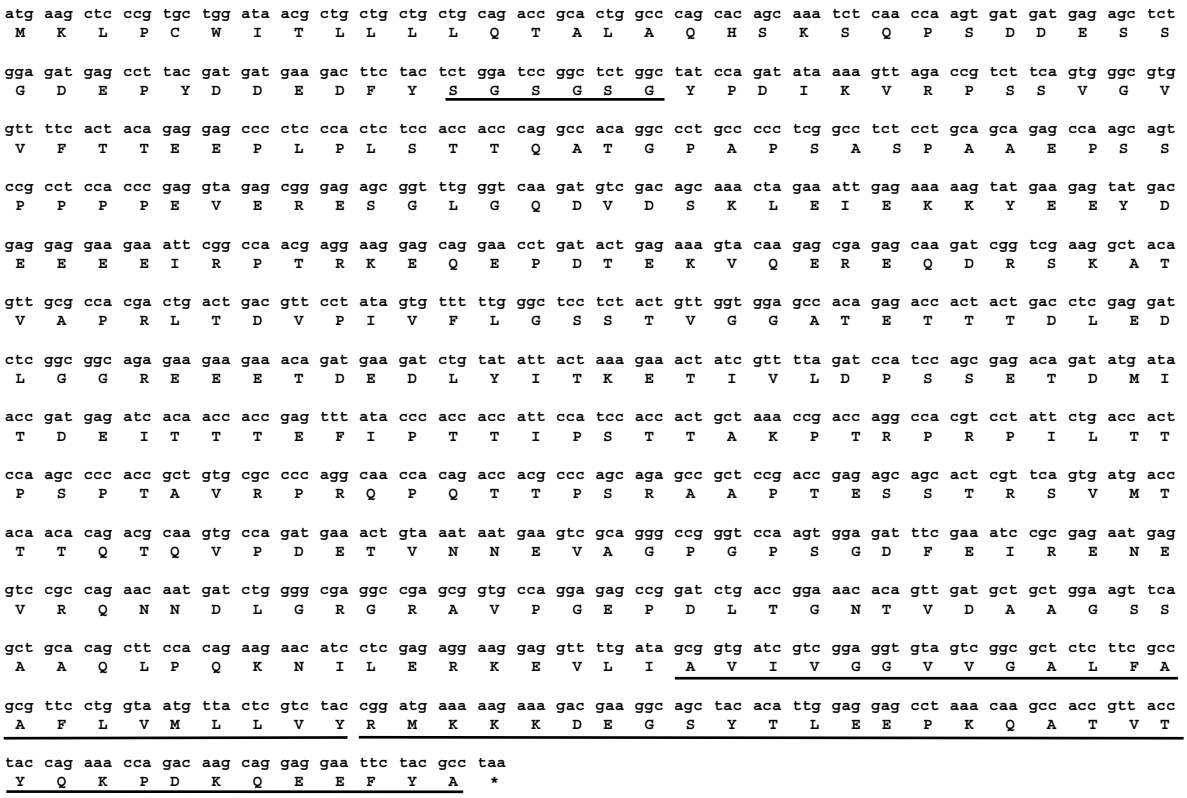

Fig. S3 cDNA and protein sequence of zebrafish syndecan-3. Regions corresponding to putative attachment sites for heparan sulfate chains and to predicted transmembrane and cytoplamic domains are underlined.

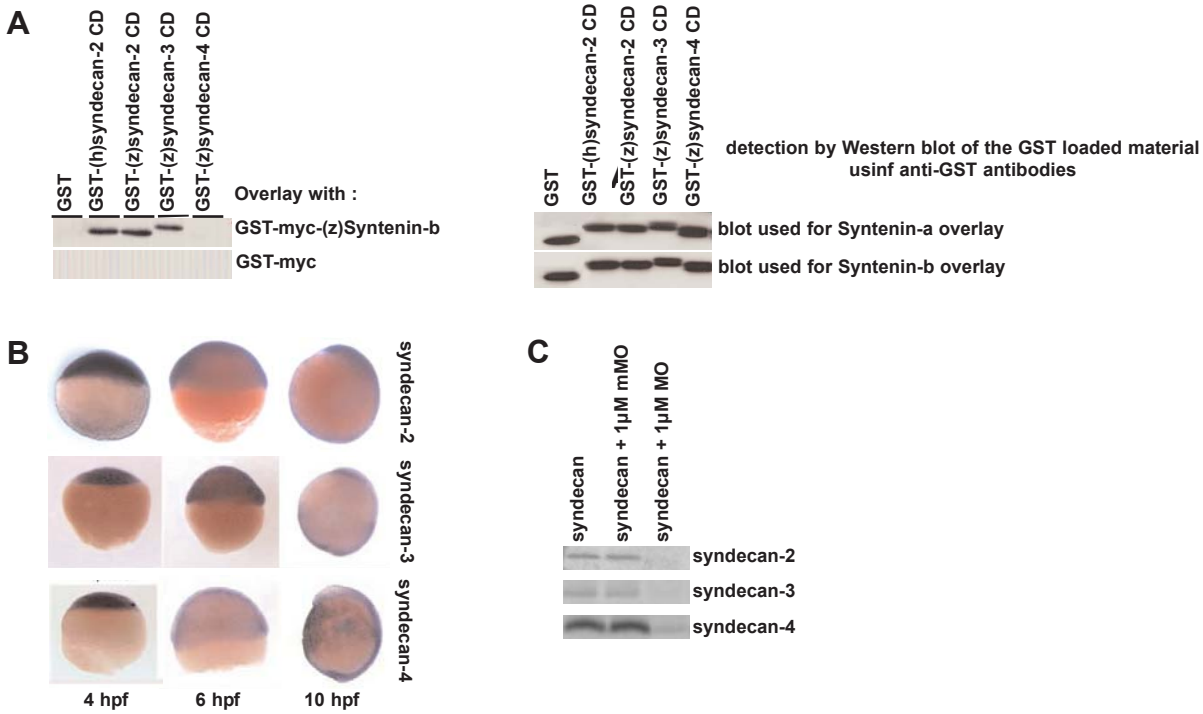

Fig. S4 (**A**) (Left) Ligand overlay illustrating the binding of GST-myc-Syntenin-b (upper panel) to various syndecan cytoplasmic domains and the absence of binding of GST-myc (lower panel). (Right) Control experiment by Western blot with anti-GST antibodies showing that similar amounts, of GST and GST-syndecan cytoplasmic domains were loaded for the overlays with GST-Syntenin-a (upper panel) or GST-Syntenin-b (lower panel). (**B**) WISH experiment showing the broad spatio-temporal expression of the different zebrafish syndecans at sphere (4 hpf), shield (6 hpf) and bud (10 hpf) stages. (**C**) In vitro transcription-translation experiment showing the activity of the MOs for the different syndecans and the ineffectiveness of their mismatch controls (mMO).